ISSN 1027-4510, Journal of Surface Investigation: X-ray, Synchrotron and Neutron Techniques, 2023, Vol. 17, Suppl. 1, pp. S28–S34. © Pleiades Publishing, Ltd., 2023.

Plasma-Assisted Vacuum Arc Deposition of Multilayer Ceramic High-Entropy Alloy Films and Their Study with Synchrotron Radiation

N. A. Prokopenko[a, *], Yu. F. Ivanov[a], N. N. Koval[a], O. V. Krysina[a], E. A. Petrikova[a], O. S. Tolkachev[a], V. V. Shugurov[a], Yu. Kh. Akhmadeev[a], V. V. Uglov[b], and A. N. Shmakov[c]

[a] *Institute of High Current Electronics, Siberian Branch, Russian Academy of Sciences, Tomsk, 634055 Russia*

[b] *Belarusian State University, Minsk, 220030 Republic of Belarus*

[c] *Budker Institute of Nuclear Physics Siberian Branch, Russian Academy of Sciences, Novosibirsk, 630090 Russia*

**e-mail: nick08_phantom@mail.ru*

Received April 29, 2023; revised June 26, 2023; accepted June 26, 2023

Abstract—The results of studies aimed at synthesizing coatings of ceramic high-entropy alloys by the vacuum-arc plasma-assisted method with simultaneous evaporation of several cathodes are presented. The optimal regimes for deposition a nitride coating of the (NbMoCrTiAl)N composition were revealed. To determine the contribution of the ion current of each arc evaporator, the azimuthal characteristics of the ion current density of the arc evaporators and the PINK-P gas plasma generator were measured. It is shown that the formed coating had a non-equiatomic composition, and the concentration of metal atoms in the coating varied from 6.6 at % up to 13.9 at %. It was established that the coating was multilayer with a layer thickness of (23–27) nm. Layers enriched in titanium atoms, alternating with layers enriched in chromium, molybdenum, and niobium atoms, were revealed. It was suggested that one of the reasons for the observed layering of the coating in terms of elemental composition was the difference in the types of crystal lattices of those elements. X-ray phase analysis was performed using synchrotron radiation, and the results of transmission electron microscopy showed that the synthesized coating had a columnar nanocrystalline structure. The transverse size of the columns varied from 20 to 170 nm, and the longitudinal size varied from 115 to 700 nm. The average crystallite size was 2.5–6 nm. The hardness of the resulting coating was 43 GPa, the friction coefficient was 0.5, and the wear parameter (a value inversely proportional to wear resistance) was 7×10^{-6} mm^3 N^{-1} m^{-1}.

Keywords: plasma-assisted vacuum arc deposition, simultaneous evaporation of several cathodes, gas-metal plasma, nitride coating, high-entropy alloy, synchrotron radiation, structure, elemental composition, phase composition, microhardness, wear resistance

DOI: 10.1134/S1027451023070418

INTRODUCTION

The first studies on the synthesis and properties of high-entropy alloys (HEAs) appeared in 2004 [1–3]. Since then, increasing interest has been shown in materials composed of five and more equiatomic elements. The composition of HEAs is widely variable, and, hence, the range of their unique properties is also wide. In particular, such alloys are resistant to corrosion [4–6], high temperatures, and oxidation [7–11], and also they have incredible mechanical characteristics [12, 13], excellent fatigue and fracture strength [12–15], and high tensile strength [16, 17].

The deposition of thin (about 1–10 μm) coatings on materials is an efficient way of improving their characteristics [18]. By now, numerous studies are available on the synthesis and deposition of thin metal and hard nitride coatings based on HEAs – HEN (high-entropy nitride). Thin coatings can be synthesized by different methods; however, the most flexible among them is plasma-assisted vacuum arc deposition, which allows one to widely vary the coating composition by varying the ion current density [19]. This plasma-assisted deposition can provide coatings with different phase states, and, thus, with different properties [20].

Our study aims to determine the optimum modes of plasma-assisted vacuum arc deposition of a (NbMoCrTiAl)N coating and to analyze its phase state, structure, and properties by different methods, including those that use synchrotron radiation.

MATERIALS AND RESEARCH TECHNIQUES

The material under study was (NbMoCrTiAl)N deposited on AISI 321 stainless steel, commercially pure Ti-Grade2 titanium, commercially pure tung-

sten, and WC-8%Co hard alloy. The gas-metal plasma for HEA nitride formation was produced by several different plasma generators operating at a time: a PINK-P gas-plasma generator based on a non-self-sustained arc discharge with thermionic and hollow cathodes and four arc evaporators with Nb (99.8 wt %), TiAl (50 wt % Al), Mo (99.96 wt %), and Cr (99.9 wt %) cathodes with a diameter of 80, 100, and 100 mm (DI80, DI100, and DI100 evaporators) and dimensions of 400 × 80 mm (DP400 evaporator), respectively. The DI100 evaporators with TiAl and Mo cathodes had improved water cooling of the cathode back surface. All plasma generators, except for the evaporator with TiAl, were located on the chamber walls around a table with "planetary satellites" at equal distances from the chamber center. The arc evaporator with TiAl was located at the top of the chamber perpendicular to the other generators.

The substrates were fixed in a holder at 45° to the satellite rotation axis for their uniform exposure to gas-metal plasmas from all generators. A detailed description of the experiment can be found elsewhere [21]. The working gas was argon and a mixture of argon with nitrogen in equal proportions; the pressure in all experiments was 0.3 Pa. Studied in the experiment were the coating growth rate and the plasma parameters provided by the separate and joint operation of the plasma sources.

The elemental composition, phase state, and defect substructure of the coatings were analyzed on a Philips SEM-515 scanning electron microscope with an EDAX ECON IV analyzer and on a JEOL JEM-2100F transmission electron microscope. Their phase state and structure were also examined on a Shimadzu XRD-6000 diffractometer (Japan) in Cu$K\alpha$ radiation and on the VEPP-3 storage ring in synchrotron radiation (INP SB RAS, Novosibirsk) under normal conditions (W substrate, radiation wavelength of λ = 0.15401 nm, and diffraction angles of $2\theta = 20°–80°$). The software was MAUD (structural analysis) and Fityk v.1.3.1 (data processing). The hardness of the coatings was measured on a PMT-3 device by the Vickers method at an indenter load of 0.5 N. Their tribological properties were studied using a pin-on-disk tribometer and oscillating TRIBOtester (TRIBOtechnic, France) with a WC-8%Co ball with a diameter of 6 mm at a load of 2 N (wear track radius of 2 mm, track length of 50 m, and ball velocity of 25 mm/s). The wear degree was determined from wear track profilometry.

RESULTS AND DISCUSSION

The contribution of the ion current of each arc evaporator was determined by measuring the azimuthal characteristics of ion current density from the evaporators and PINK-P generator (Fig. 1). The collector was located on a planetary satellite moving along the perimeter of the working chamber so that its spacing from each generator was the same. The minimum distance between the collector and generator exit aperture was 16 cm, and its maximum value was 52 cm. In all experiments, the pressure of the gas mixture of argon with nitrogen was 0.3 Pa, while the partial pressure of nitrogen was 0.15 Pa.

The measurements show that when each plasma generator operates separately, the ion current density decreases monotonically with distance from the generator exit aperture irrespective of the discharge current (Figs. 1a–1e). During such operation, the ion current from each generator is present even at the most distant point.

From the azimuthal ion current density distribution measured with separately operating plasma generators (Figs. 1a–1e), we determined the arc parameters at which the average densities of the ion current from all evaporators to the collector were were the same and were 2.45 mA/cm^2. This provides the most uniform ion current density over the chamber during the simultaneous operation of the generators. Thus, the discharge currents of the plasma generators for the deposition of high-entropy nitride (HEN) coatings were the following: I_{TiAl} = 180 A, I_{Mo} = 90 A, I_{Cr} = 150 A, I_{Nb} = 120 A, and I_{PINK} = 50 A.

The azimuthal distribution of the ion current density during the simultaneous operation of all plasma generators (Fig. 1f) demonstrates that its value measured is 6.3–10 mA/cm^2 depending on the position of the collector in the chamber and the distance from the PINK-P generator. During the joint operation of the generators, compared to their separate operation, the density of the ion current to the substrates is more uniform, and this provides a constant temperature throughout the deposition and a uniform HEA layer thickness.

In a series of experiments, we determined the growth rates of nitride coatings and HEN coatings with separately and jointly operating plasma generators, respectively. The arc currents were set so that the ion current densities for all evaporators were about equal. In all experiments, the holder with WC-8%Co substrates was located 16 cm from the generator exit aperture. To determine the growth rate of HEN, the holder was located on a planetary satellite moving along the chamber perimeter at 2.5 rpm. The negative substrate bias was –50 V; the deposition time for all coatings was 60 min. The coating thickness was measured by the Calotest method. The coating growth rates are presented in Table 1. As can be seen, the growth rate of (NbMoCrTiAl)N is higher than those of TiAlN, MoN, NbN, and CrN but is markedly lower than the sum of these rates. This is associated with high densities of the ion current to the substrate during the simultaneous operation of the generators and with ion plasma etching of the growing HEN coating.

A HEN coating with a thickness of 3 μm is considered further. According to the X-ray diffraction data,

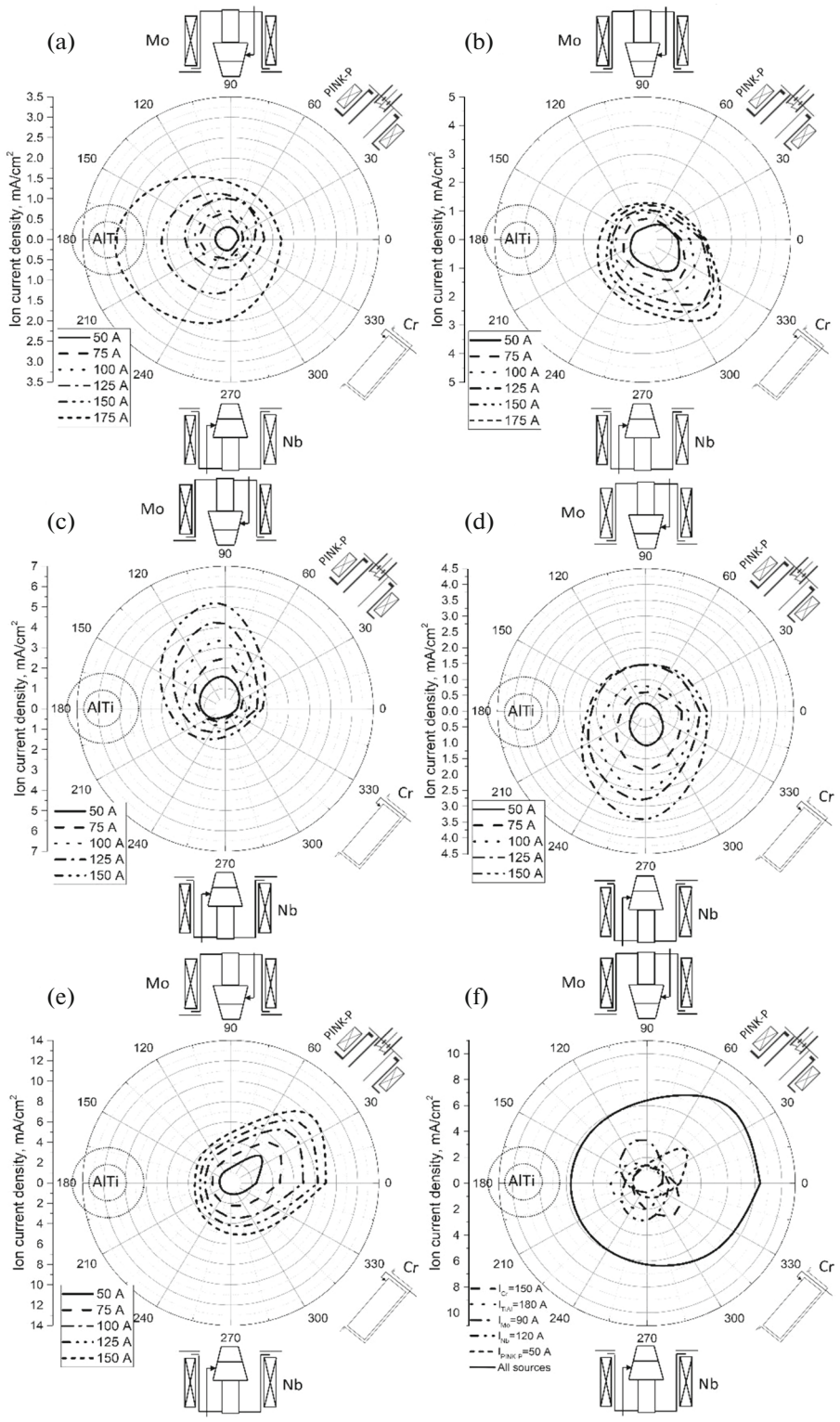

Fig. 1. Azimuthal ion current density distribution vs arc current for different plasma generators with different cathode materials: (a) DI100, TiAl, (b) DP400, Cr, (c) DI100, Mo, (d) DI80, Nb, (e) PINK-P, (f) joint operation of all plasma generators.

the coating contains nitrogen atoms and metal atoms from the cathode materials, suggesting the formation of (NbMoCrTiAl)N (Fig. 2).

According to transmission and scanning transmission electron microscopy, the HEN coating is a multilayer film with visually alternating dark and bright lay-

Table 1. Growth rates of nitride coatings

Coating material	TiAlN	MoN	NbN	CrN	(NbMoCrTiAl)N
Discharge current, A	180	90	120	150	
Coating growth rate, μm/h	5.2	1.4	2	2.4	6

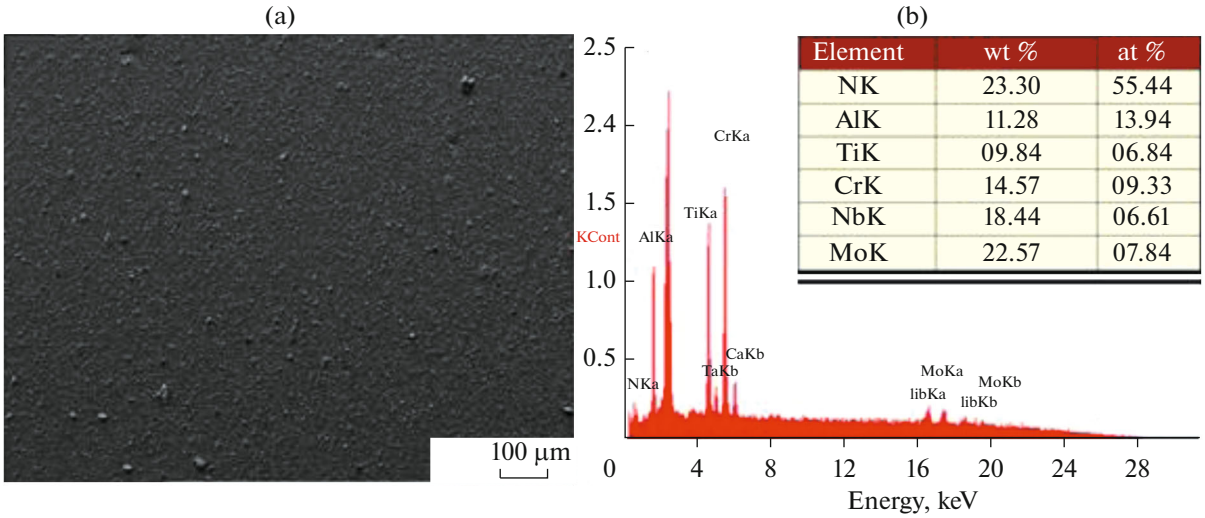

Fig. 2. Surface of the HEN coating, scanning electron microscopy (a), respective energy spectra (b), and coating composition (inset).

ers (Fig. 3). The average thickness of the dark and bright layers is ≈27 and 23 nm, respectively.

Our X-ray diffraction analysis of the coating shows that its layers rich in Ti alternate with those rich in Cr, Mo, and Nb (Fig. 4). Such alternation in the coating composition may be governed, among other things, by different lattice types of its elements: hexagonal close-packed (hcp) Ti and body-centered cubic (bcc) Cr, Mo, and Nb. The signals of N and Al atoms are too weak for their reliable analysis.

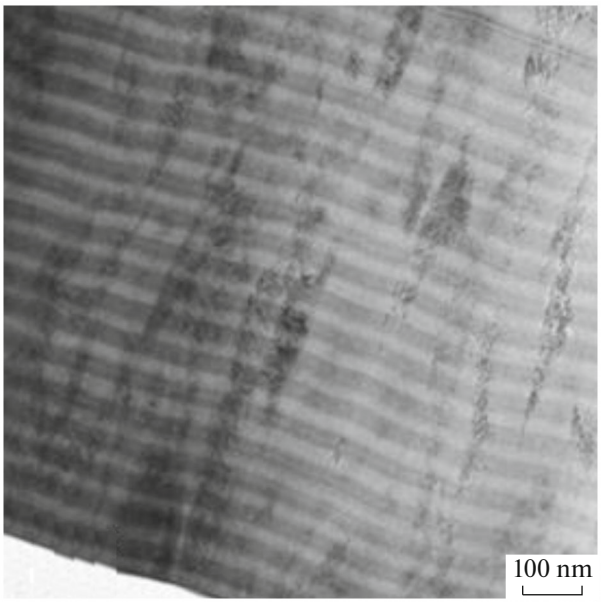

Fig. 3. Structure of the (NbMoCrTiAl)N coating. Transmission electron microscopy.

The data on transmission electron microscopy also suggest that the ceramic coating has a columnar structure (Fig. 5). The transverse size of the columns ranges from 20 to 170 nm, and their longitudinal size ranges from 115 to 700 nm. The columns have a nanocrystalline structure with a crystallite size of 2.5–6.0 nm (Fig. 5d). The electron diffraction pattern of the coating corresponds in interplanar spacings to face-centered cubic crystal (fcc) lattice (Fig. 5b).

The X-ray diffraction pattern of the coating on a W plate in synchrotron radiation reveals a broad peak (Fig. 6), suggesting that the film is X-ray amorphous or finely dispersed. This result, along with the data on transmission electron microscopy, points to the nanocrystalline state of the material.

The average hardness of the high-entropy nitride coating on a WC-8%Co substrate is 43 GPa. It should be noted that the hardness of the coating essentially depends on many factors: elemental composition, manufacturing method, texture, phase composition, etc. Examples of HEN coatings with very high hardness formed by ion plasma methods are

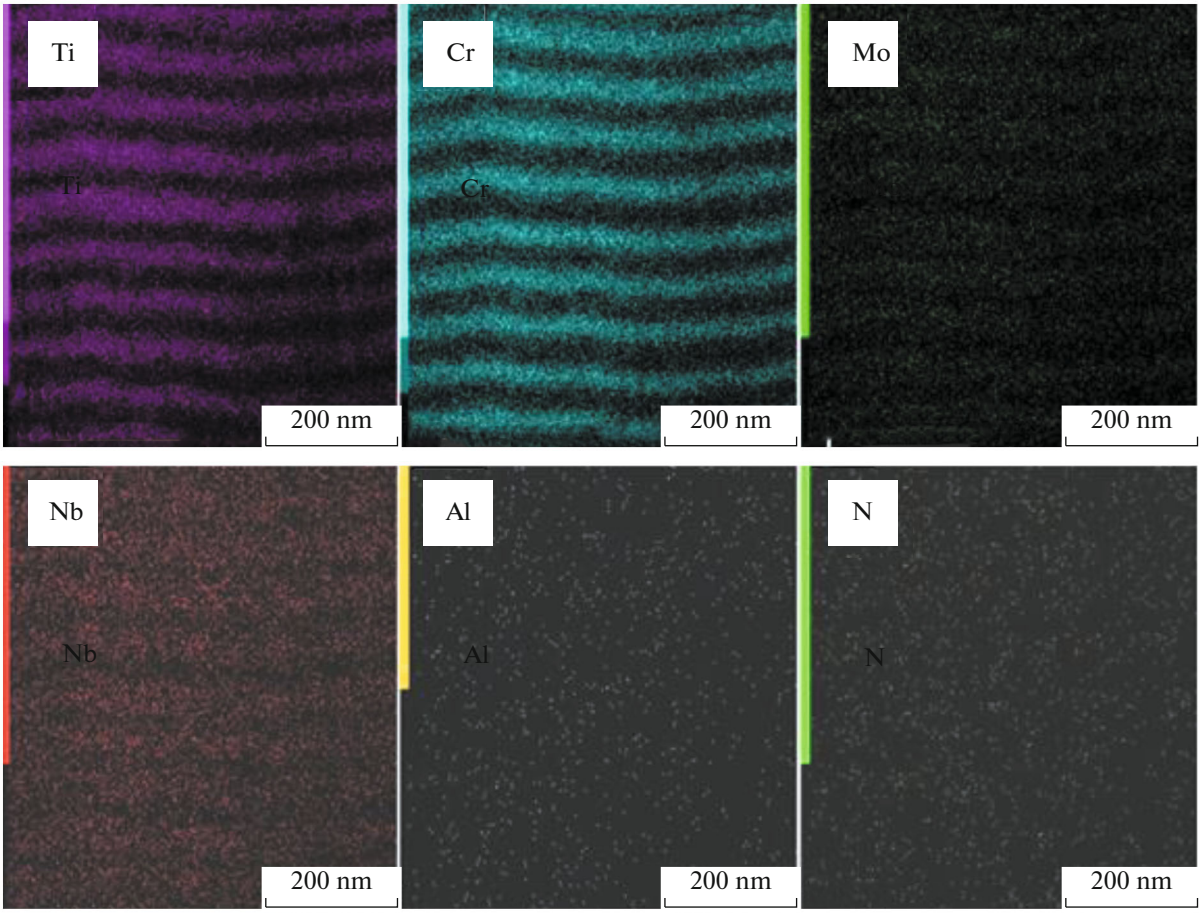

Fig. 4. Structure of the HEN coating in characteristic X-rays from Ti, Cr, Mo, Nb, Al, and N atoms.

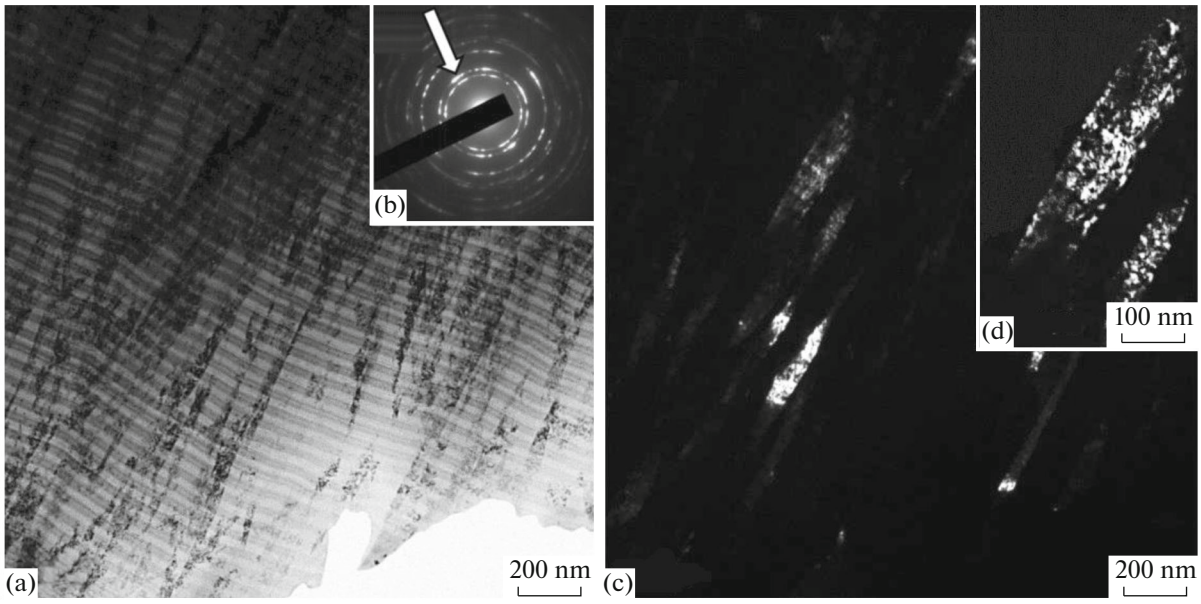

Fig. 5. Structure of the (NbMoCrTiAl)N coating: bright field (a), electron diffraction pattern (b), and dark field in [002] reflection (c, d) shown by an arrow in (b). Transmission electron microscopy.

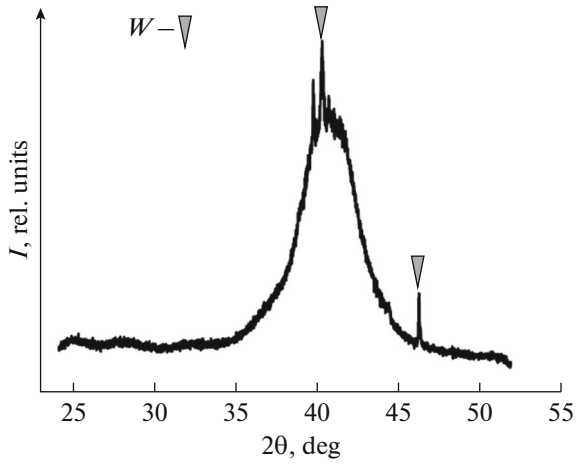

Fig. 6. Fragment of the X-ray diffraction pattern of the HEN coating on a W plate in synchrotron radiation.

(AlCrTiVZr)N – 42 GPa [22], (TiZrNbAlYCr)N – 47 GPa [23], and (TiHfZrVNb)N – 65 GPa [24]. Its specific wear rate, which is inversely proportional to wear resistance, is 7×10^{-6} mm^3 H^{-1} m^{-1}. The friction coefficient of the coatings varies from 0.45 to 0.50.

CONCLUSIONS

Our study on the deposition of (NbMoCrTiAl)N coatings, including the azimuthal characteristics of arc discharges with singly and jointly operating plasma generators, shows that the average density of the ion current from each evaporator for optimum coating deposition is 2.45 mA/cm^2. The sum of the growth rates of TiAlN, MoN, NbN, and CrN coatings is not equal to the growth rate of (NbMoCrTiAl)N. The (NbMoCrTiAl)N coating with a thickness of 3 μm represents a multilayer film. According to the data of X-ray diffraction analysis in synchrotron radiation and of transmission electron microscopy, the (NbMoCrTiAl)N coating has a nanocrystalline structure with a crystallite size of 2.5–6 nm, where the crystallites form columns with average longitudinal and transverse sizes of 285 and 60 nm, respectively. The high-entropy nitride coating features superhardness (43 GPa) and relatively high wear resistance, which makes the coating promising for use in industry.

FUNDING

The work was supported by the Ministry of Science and Higher Education of the Russian Federation under project no. 075-15-2021-1348 within the framework of event nos. 3.1.4, 3.1.5, 3.1.12 and 3.1.13. TEM equipment was provided by Tomsk Polytechnic University (Collective Use Center Innovative Center for Nanomaterials and Nanotechnology, Tomsk Polytechnic University) under RF MES project no. 075-15-2021-710.

CONFLICT OF INTEREST

The authors of this work declare that they have no conflicts of interest.

REFERENCES

1. B. Cantor, I. T. H. Chang, P. Knight, and A. J. B. Vincent, Mater. Sci. Eng., A **375**, 213 (2004). https://doi.org/10.1016/j.msea.2003.10.257
2. J.-W. Yeh, US Patent No. 20020159914A1 (2002).
3. J.-W. Yeh, S.-K. Chen, S.-J. Lin, J.-Y. Gan, T.-S. Chin, T.-T. Shun, C.-H. Tsau, and S.-Y. Chang, Adv. Eng. Mater. **6**, 299 (2004). https://doi.org/10.1002/adem.200300567
4. Q. Wang, A. Amar, C. Jiang, H. Luan, S. Zhao, H. Zhang, G. Le, X. Liu, X. Wang, X. Yang, and J. Li, Intermetallics **119**, 106727 (2020). https://doi.org/10.1016/j.intermet.2020.106727
5. H. Zhang, W. Li, H. Xu, L. Chen, J. Zeng, Z. Ding, W. Guo, and B. Liu, Coatings **12**, 628 (2022). https://doi.org/10.3390/coatings12050628
6. P. Das, R. Nandan and P. M. Pandey, Trans. Indian Inst. Met. **75**, 2465 (2022). https://doi.org/10.1007/s12666-022-02610-9
7. V. G. Khyzhniak, T. V. Loskutova, O. E. Datsyuk, I. S. Pohrebova, N. A. Kharchenko, T. P. Hovorun, A. I. Dehula, I. Ya. Smokovich, and Ya. O. Kravchenko, High Temp. Mater. Processes **20**, 267 (2016). https://doi.org/10.1615/HighTempMatProc.2017019326
8. L. R. Kanyane, N. Malatji, A.P.I Popoola, and O.S.I. Fayomi, Results Phys. **14**, 102465 (2019). https://doi.org/10.1016/j.rinp.2019.102465
9. Y. D. Wu, Y. H. Cai, T. Wang, J. J. Si, J. Zhu, Y. D. Wang, and X. D. Hui, Mater. Lett. **130**, 277 (2014). https://doi.org/10.1016/j.matlet.2014.05.134
10. Y. Zou, H. Ma, and R. Spolenak, Nat Commun. **6**, 7748 (2015). https://doi.org/10.1038/ncomms8748
11. A. D. Pogrebnjak, O. V. Bondar, I. V. Yakushchenko, C. Kozak, and K. Czarnacka, High Temp. Mater. Processes **19**, 257 (2015). https://doi.org/10.1615/HighTempMatProc.2016016169
12. M.-H. Chuang, M.-H. Tsai, W.-R. Wang, S.-J. Lin, and J.-W. Yeh, Acta Mater. **59**, 6308 (2011). https://doi.org/10.1016/j.actamat.2011.06.041
13. M. A. Hemphill, T. Yuan, G. Y. Wang, J. W. Yeh, C. W. Tsai, A. Chuang, and P. K. Liaw, Acta Mater. **60**, 5723 (2012). https://doi.org/10.1016/j.actamat.2012.06.046
14. Z. Tang, T. Yuan, C.-W. Tsai, J.-W. Yeh, C. D. Lundin, and P. K. Liaw, Acta Mater. **99**, 247 (2015). https://doi.org/10.1016/j.actamat.2015.07.004
15. B. Gludovatz, A. Hohenwarter, D. Catoor, E. H. Chang, E. P. George, and R. O. Ritchie, Science **345**, 1153 (2014). https://doi.org/10.1126/science.1254581
16. Y. Deng, C. C. Tasan, K. G. Pradeep, H. Springer, A. Kostka, and D. Raabe, Acta Mater. **94**, 124 (2015). https://doi.org/10.1016/j.actamat.2015.04.014

17. D. Li, C. Li, T. Feng, Y. Zhang, G. Sha, J. J. Lewandowski, P. K. Liaw, and Y. Zhang, Acta Mater. **123**, 285 (2017). https://doi.org/10.1016/j.actamat.2016.10.038

18. D. M. Mattox, *The Foundations of Vacuum Coating Technology*, 2nd ed. (Elsevier, Amsterdam, 2018)

19. O. V. Krysina, N. A. Prokopenko, Yu. F. Ivanov, O. S. Tolkachev, V. V. Shugurov, and E. A. Petrikova, Surf. Coat. Technol. **393**, 125759 (2020). https://doi.org/10.1016/j.surfcoat.2020.125759

20. O. V. Krysina, N. N. Koval, S. S. Kovalsky, V. V. Shugurov, I. V. Lopatin, N. A. Prokopenko, and E. A. Petrikova, Vacuum **187**, 110123 (2021). https://doi.org/10.1016/j.vacuum.2021.110123

21. Yu. F. Ivanov, N. N. Koval, Yu. H. Akhmadeev, V. V. Uglov, V. V. Shugurov, E. A. Petrikova, O. V. Krysina, N. A. Prokopenko, and I. I. Azhazha, Russ. Phys. J. **64**, 32 (2021). https://doi.org/10.17223/00213411/64/12/32

22. Y. Xu, G. Li, and Y. Xia, Appl. Surf. Sci. **523**, 146529 (2020). https://doi.org/10.1016/j.apsusc.2020.146529

23. A. D. Pogrebnjak, V. M. Beresnev, K. V. Smyrnova, Y. O. Kravchenko, P. V. Zukowski, and G. G. Bondarenko, Mater. Lett. **211**, 316 (2018). https://doi.org/10.1016/j.matlet.2017.09.121

24. S. A. Firstov, V. F. Gorban, N. I. Danilenko, M. V. Karpets, A. A. Andreev, and E. S. Makarenko, Powder Metall. Met. Ceram. **52**, 560 (2014). https://doi.org/10.1007/s11106-014-9560-z